Analysis of the Stratospheric Aerosol Load After the 2019 Raikoke Eruption

Felicia Carlborg

Bachelor of Physics
January 2021

LUND
UNIVERSITY

Department of Physics
Division of Nuclear Physics

Supervisor: Johan Friberg
Co-supervisor: Carl Svenhag

Project duration: 3/9/20 - 14/12/20

Popular Scientific Summary

Today it is well known that greenhouse gases emitted by mankind contribute to global warming. What is less known to the general public is that major volcanic eruptions can lead to global cooling. Volcanic eruptions do not only emit ash, but they also emit sulfur dioxide. When this gas gets emitted straight into the higher atmosphere (i.e. the stratosphere), it turns into sulfate particles that act as a shield against incoming solar radiation. If the eruption is strong enough this might lead to global cooling. For example, in 1991 there was a major eruption of Mount Pinatubo that caused cooling of the global climate years after the eruption.

Climate models have been bad at representing these particles and their cooling properties. Therefore, the global warming has been overestimated, and as a result, the contribution by greenhouse gases has been underestimated. Hence, studying volcanic aerosols and their radiative properties are crucial to fully understand climate change.

In this project the stratospheric volcanic aerosols after the eruption of the Raikoke volcano in 2019 have been investigated. This has been done using satellite data from the CALIPSO satellite that was launched in 2006 by NASA and CNES. The goal was to see how the eruption affected the stratosphere and its radiative properties.

Abstract

The stratospheric aerosol load after the eruption of Raikoke in 2019 have been analysed with satellite data from the CALIPSO satellite. The goal was to see how much the stratospheric aerosol load increased due to the Brewer Dobson circulation, and further, how this affected the stratospheric aerosol optical depth (AOD), and the corresponding radiative forcing (RF). This was done by performing a data analysis of the backscattering data retrieved from the CALIPSO satellite. The results showed a doubling of the stratospheric aerosol load six months after the eruption, an increase in the stratospheric AOD, and decrease in the RF in the northern hemisphere. The peak AOD found was 0.02 which occurred three months after the eruption, and the corresponding peak value of the RF was -0.5 W/m^2. When compared to similar eruptions such as Sarychev 2009, it was assumed that the stratospheric aerosol load went back to normal conditions after one year, since only six months after the eruption were studied in this analysis. Hence, it could be concluded that the eruption increased the stratospheric aerosol load in the northern hemisphere, and therefore affected the climate. This showed that future work, including analysis of the stratosphere after volcanic eruptions, is important to understand the impact it has on the climate.

Keywords: Volcanic Climate Impact, Raikoke, CALIPSO, Satellite, Stratospheric Aerosols, Radiative Forcing, Aerosol Optical Depth

Contents

Acknowledgements

First of all, I would like to thank my supervisor Johan Friberg and co-supervisor Carl Svenhag for always helping me with any problem, and especially for being able to solve problems on Zoom during these special times. I would also like to thank you for your enthusiasm, and for introducing me to this exciting field in science. I would also like to thank the rest of the staff at the division for being able to help me when my supervisors were not around.

Also, I would like to thank Carl Gustafsson for help with the programming and for mental support during the writing of this thesis. Thank you especially for teaching me how to properly read the error messages, and to not give up on the first try.

Lastly, I would like to thank my friends and family for the love and support during this semester, and throughout my entire education. Without any of you, I would not be where I am today.

Acronyms

AOD	Aerosol Optical Depth
AS	Aerosol Scattering
CALIPSO	Cloud-Aerosol Lidar and Infrared Pathfinder Satellite Observation
CALIOP	Cloud Aerosol Lidar with Orthogonal Polarization
GloSSAC	Global Space-based Stratospheric Aerosol Climatology
GMAO	Global Modeling and Assimilation Office
CMIP5	Coupled Model Intercomparison Project 5
LMS	Lowermost Stratosphere
MERRA-2	Modern-Era Retrospective analysis for Research and Applications, Version 2
NH	Northern Hemisphere
PSC	Polar Stratospheric Cloud
RF	Radiative Forcing
RMS	Root Mean Square
SAA	South Atlantic Anomaly
SH	Southern Hemisphere
SR	Scattering Ratio
VEI	Volcanic Explosivity Index

1 Introduction

It is well known that anthropogenic greenhouse gases contribute to increased global warming. On the other hand, there are also aerosols that contribute to a cooling of the climate. For example, during volcanic eruptions great amounts of sulfur dioxide are emitted into the atmosphere (Solomon et al., 2011). If the eruption is strong enough, it might get injected directly into the stratosphere where it can stay for months up to several years (Kremser et al., 2016). It can prevail in the stratosphere for a long time because of a circulation called the Brewer Dobson-circulation. Additionally, in the stratosphere, the sulfur dioxide transforms into sulfate aerosols which scatter incoming shortwave solar radiation (Kremser et al., 2016; Sheng et al., 2015). One example of when the global temperature cooled was after the eruption of Mount Pinatubo in 1991, when the global temperature cooled with about 0.5°C (McCormick, Thomason, and Trepte, 1995). Strong tropical eruptions are thought to contribute the most to the cooling since the Brewer Dobson circulation transport particles from the tropics to both hemispheres. However, satellite data have shown that smaller eruptions might affect the stratospheric aerosol burden more than once thought (Solomon et al., 2011).

The cooling effect of these aerosols has probably masked the global warming caused by greenhouse gases (Ramanathan and Feng, 2008). Hence, if this climate forcing is neglected in climate models, the forcing caused by greenhouse gases might get underestimated. For example, in the fifth phase of the Coupled Model Intercomparison Project (CMIP5), the global warming was overestimated in nearly all climate models. One of the reasons might have been that the simulations did not account for the volcanic aerosol loadings after 2000 (Andersson et al., 2015). However, according to IPCC (2013), aerosols and its interaction with clouds, and radiative properties, constitutes a large part of the uncertainty in today's climate models.

This study aims to analyse the change in the stratospheric aerosol load after the eruption of Raikoke, located in Russia, that erupted in June 2019. This eruption would be considered a smaller eruption compared to the one of Pinatubo, and is situated at the midlatitudes. The results were then compared to historical eruptions to see if the eruption had any effect on the stratosphere and climate. The nadir viewing CALIPSO satellite was used for this project since it has high vertical resolution compared to previous used limb viewing satellite instruments. This way the whole stratospheric column was analysed including the lowermost stratosphere (LMS), which constitutes over 40 % of the stratospheric aerosol load (Andersson et al., 2015).

2 Background

2.1 The Raikoke Eruption

On June 21st 18.05 UTC, the midlatitude volcano Raikoke erupted for the first time in 95 years. There were a total of 9 explosions where 6 of them occurred during the first 25 minutes (Global Volcanism Program, 2019b). The volcano is located on Raikoke island and is part of the Kuril Islands in the sea of Okhotsk in Russia (Global Volcanism Program, 2013). The ash plumes reached 10-13 km in altitude (i.e. the stratosphere), and contained a large amount of sulfur dioxide. These drifted east and north-east since a cyclone forced the material this direction. On June 23 local time, the plume had drifted 2000 km east-north-east. There were also significantly strong explosions June 22nd 05.40 UTC that caused ash plumes with an altitude of 10-11 km. The explosions continued until approximately June 22nd 08.00 UTC (Global Volcanism Program, 2019b). The volcanic explosivity index (VEI) of the eruption was 3 (Global Volcanism Program, 2020), which is a relative measure of the explosiveness of a volcanic eruption (Newhall and Self, 1982).

Five days after the eruption of Raikoke, the tropical volcano Ulawun erupted, and was active until 5th of October 2019. The largest plumes of 19.2 km occurred at the end of June and beginning of August (Global Volcanism Program, 2019e; Global Volcanism Program, 2019d). No data could be found on the total amount of emitted sulfur dioxide. However, when comparing the sulfur dioxide emissions on NASA Worldview (NASA, 2020b), Raikoke emitted a considerable amount more sulfur dioxide than Ulawun. Nonetheless, this volcano might have also had a considerable effect on the stratospheric aerosol load, which will be discussed further.

2.2 The Atmosphere

The atmosphere contains different layers based on its vertical temperature profile. The first layer is the troposphere where all the weather events take place. The air temperature in this layer decreases with height, and is well mixed with rising and descending air currents. The next layer is called the stratosphere, and its vertical temperature profile increases with height. The boundary separating these two is called the tropopause. The height of this layer varies, but is generally higher in summer at all latitudes, and highest at the equator. This boundary, and the temperature inversion in the stratosphere, inhibits the vertical currents from the troposphere to transmit into

the stratosphere. The reason for the stratospheric temperature inversion is because of ozone in the stratosphere, which absorbs UV light from the sun and heats the stratosphere (Ahrens and Henson, 2016).

Even so, transport between the troposphere and stratosphere occurs. The lowermost stratosphere (LMS), which lies between the tropopause and the overlying 380 K isentrope (a plane with constant potential temperature), is connected with the tropical troposphere through isentropic surfaces. Exchange can either occur along the isentropic surface adiabatically, or diabatically across the isentropic surfaces (Holton et al., 1995). Transport between the troposphere and stratosphere is also connected via the Brewer-Dobson circulation which is a meridional circulation that transports upwelling air from the tropics to the midlatitudes and polar regions (Butchart, 2014), which will be explained further in section 2.3.

At around 50 km altitude, the stratopause separates the stratosphere from the mesosphere. Below this level, around 99.9 % of the atmospheric mass is located. Thus, the air in the mesosphere is very thin. The vertical temperature profile in the mesosphere is decreasing with height due to the low amount of ozone. The last of the vertical layers is the thermosphere. It is separated with the mesosphere by the mesopause. The thermosphere contains oxygen molecules which absorb solar radiation that warms the air. Hence, the vertical temperature profile in this layer increases with height. At around 500 km altitude the molecules have a mean free path of around 10 km. Here, the light molecules can escape the Earth's gravitational pull into space. This region is sometimes called the exosphere and it is the top of the thermosphere (Ahrens and Henson, 2016).

2.3 The Brewer-Dobson Circulation

The Brewer-Dobson circulation is a meridional circulation that transports upwelling air from the tropics to the midlatitudes and polar regions. It consists of shallow and deep branches (Birner and Bönisch, 2011), which are shown in figure 1. The shallow branches extend into the low stratosphere to 70 hPa and are then transported to the midlatitudes, whereas the deep branches start above 70 hPa which extends from the tropics through the middle atmosphere to the midlatitudes (Kremser et al., 2016). This means that air in the deep branches is transported slowly, and the residence time of the suspended particles can remain up to several years (Birner and Bönisch, 2011). When the particles reach the midlatitudes and the polar regions, the aerosols get transported to the troposphere. Here, the aerosols are deposited

by wet and dry deposition (Kremser et al., 2016). Since the air in the shallow branches only extends to lower altitudes, it takes a year or less for the particles to transport to the midlatitudes. Additionally, the shallow branches have lower seasonality, while the deep branches are stronger in the winter hemisphere (Birner and Bönisch, 2011).

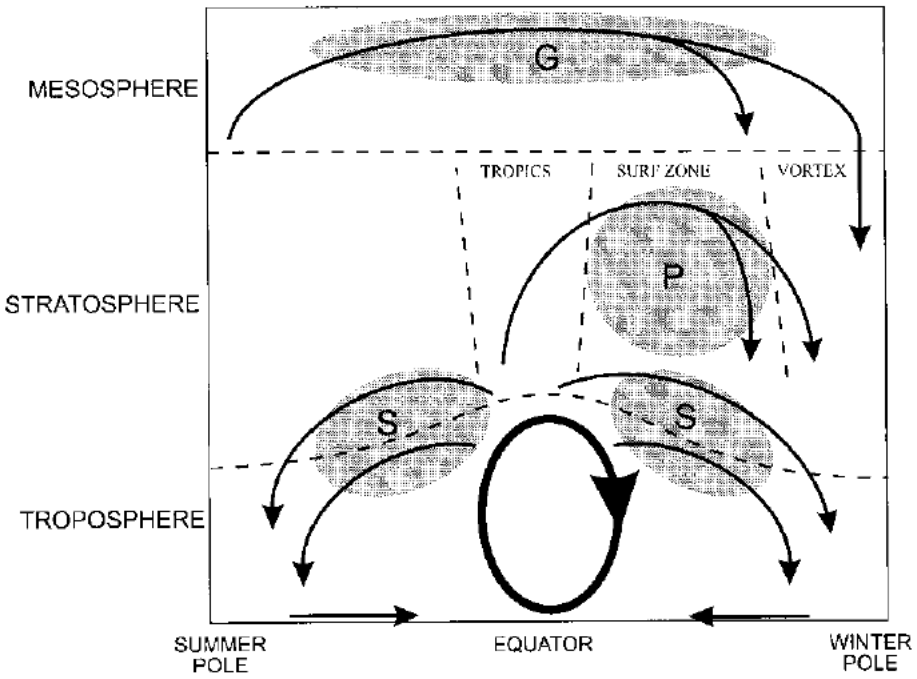

Figure 1: The arrows represent the meridional transports in the different layers of the atmosphere. The shallow branches can be seen close to the tropopause (lower dashed lines), and the deep branches start above the tropopause and extend into the winter hemisphere. The gray areas show where the induced wave-drag occurs (P = planetary waves, S = synoptic scale waves, G = gravity-inertia waves). The circulation in the middle represents the Hadley cell which is driven thermally (Plumb, 2002). The figure is retrieved from Plumb (2002).

The underlying driving force for the deep branches is the "extratropical pump" or "Rossby wave-pump" (Butchart, 2014). Rossby waves are planetary waves with a wavelength of thousands of kilometers that encircle the Earth. (Ahrens and Henson, 2016). When these waves propagate vertically from the troposphere and dissipate, they induce a non-local wave-drag that causes air to ascend in the tropics and descend in the midlatitudes (Butchart, 2014). The wave breaking also causes stirring air across the isentropes within

the so called "surf zone" (see figure 1). Consequently, there is a two-way horizontal mixing across the isentropes (Plumb, 2002; Butchart, 2014). Since the drag from the Rossby waves can only be westward - the pumping can only go in the poleward direction to conserve angular momentum. (Butchart, 2014). Similarly, the shallow branches are driven by vertically propagating synoptic scale waves, and there is also a meridional transport in the mesosphere extending from the summer pole to the winter pole that in the same manner is driven by vertically propagating gravity-inertia waves (Plumb, 2002).

2.4 Stratospheric Aerosols

When particles and sulfur-containing gases enter the stratosphere, stratospheric aerosols are formed through chemical reactions and microphysical processes. Both natural, such as volcanic eruptions, and anthropogenic emissions of sulfur-containing gases contribute to the stratospheric aerosol burden (Sheng et al., 2015). However, Neely et al. (2013) did simulations of anthropogenic emissions and volcanic emissions from 2000-2010, and compared to satellite observations. The conclusion was that moderate volcanic emissions were the main source of stratospheric aerosols during this period.

In an explosive volcanic eruption, sulfur dioxide gets emitted straight into the stratosphere. There, it transforms into sulfuric acid (H_2SO_4), which when reacted with water, turns into sulfate aerosols. (Kremser et al., 2016). Sulfate and other stratospheric aerosols scatter solar radiation, and absorb outgoing infrared radiation (Sheng et al., 2015). The net imbalance in the radiative energy budget that this is causing is called radiative forcing. More specifically, radiative forcing is the perturbation in the radiative budget for the Earth system, caused by e.g increased cloud cover, greenhouse gases or aerosols. Sulfate aerosols will induce negative radiative forcing, since the increased sulfate mass will perturb the system with more outgoing radiation. Carbon dioxide and other greenhouse gases do the opposite. Their increased mass will perturb the system by keeping more radiation inside the Earth system. This change in the radiative energy budget affects the surface temperature (Jacob, 1999). Section 2.7 shows a relation of how to retrieve the radiative forcing.

After the eruption of Mt Pinatubo 1991, the net radiative forcing decreased with about -4 W/m^2 (Kremser et al., 2016). That caused the global temperature to decrease with about 0.5 °C years after the eruption (McCormick, Thomason, and Trepte, 1995). This eruption emitted approximately 18-19 Tg of sulfur dioxide into the atmosphere according to Guo et al. (2004), while

an estimation by Global Volcanism Program (2019c) suggests that only 1.4-1.5 Tg sulfur dioxide were emitted during the Raikoke eruption.

There has not been a major eruption since Pinatubo 1991. However, several smaller eruptions have, according to Solomon et al. (2011), contributed to an increase in the stratospheric aerosol load by about 7 % per year between 2000 - 2010. This has induced a decrease in global radiative forcing of about -0.1 W/m^2. Further, the same study showed that this has slowed down the global warming that otherwise would have occured.

Volcanic aerosols injected directly into the stratosphere in the midlatitudes, and higher latitudes, stay in the stratosphere for months before being deposited in the troposphere in the same hemisphere. When injected into the stratosphere above 20 km in the tropics, the aerosols go into the deep Brewer-Dobson branch and can stay in the stratosphere for years. The eruption of the tropical volcano El Chichón 1983 is an example of when the volcanic aerosols stayed in the stratosphere for many years before they deposited in both hemispheres (Kremser et al., 2016).

During extratropical eruptions it also depends on how high in the stratosphere the sulfur dioxide gets injected. In a study by Friberg et al. (2018), it was concluded that emissions injected close to the extratropical tropopause only increased the stratospheric aerosol load temporarily. If the sulphur dioxide was emitted into the LMS, the aerosols stayed there and affected the stratospheric aerosol load for under a year. Emissions injected above the LMS (380 K - 470 K) spread horizontally across the lower Brewer-Dobson branch, over the entire hemisphere to the tropics, and affected the stratospheric aerosol load up to a year. For example, Sarychev that erupted in 2009 had this effect on the stratospheric aerosol load in the northern hemisphere (Friberg et al., 2018).

2.5 CALIPSO Satellite

The satellite data for this project were retrieved from the nadir viewing (in the vertical) lidar instrument CALIOP aboard the CALIPSO satellite. It launched in 2006 and is a collaboration between NASA and CNES (the French space agency) (Winker et al., 2010). Before CALIOP, satellite remote sensing had a limited ability of studying the vertical resolution of aerosols and clouds. This is because limb viewing (in the horizontal) instruments have been used historically to analyse the stratospheric aerosol load, and they had a hard time measuring aerosols close to the tropopause because of

clouds and thick volcanic clouds. Therefore, these instruments made it hard to measure the LMS (Andersson et al., 2015).

CALIOP has a two-wavelength laser transmitter (532 nm and 1064 nm) and a three channel receiver. One channel receives the attenuated backscattering at 1064 nm, and two channels receive the parallel, and perpendicular polarized attenuated backscattering at 532 nm (Winker et al., 2010). A 1 m diameter telescope is also attached to the instrument which collects the backscattered signals (Winker et al., 2009). A schematic picture of the CALIOP instrument is shown in figure 2.

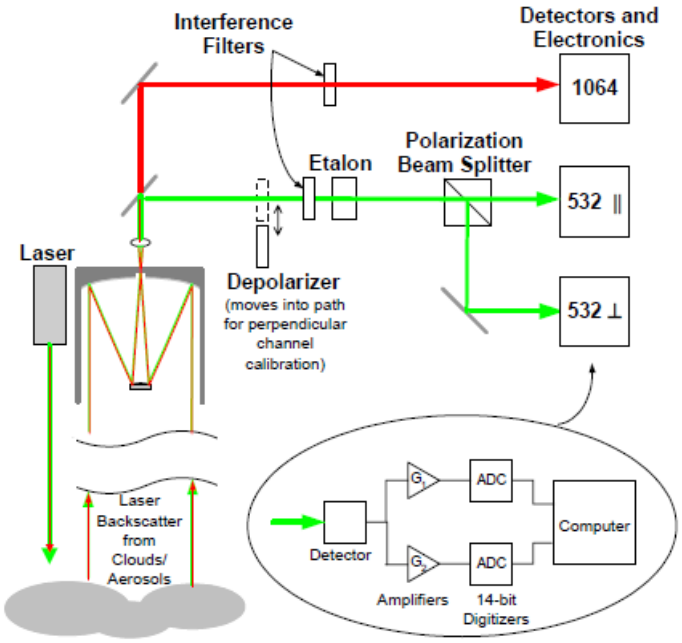

Figure 2: Schematic picture of the CALIOP instrument onboard CALIPSO. The backscattered light is collected by a telescope, which is then transferred through interference filters (and an etalon for the 532 beam), which reduces the solar background before going into the detectors. After detection the signals are digitized by an ADC (Analog-to-Digital-Converter), which can be seen in the circle (Winker et al., 2009). The figure is acquired from Hostetler et al. (2006).

The satellite is situated 705 km above Earth in a sun synchronous polar orbit, collects data between 82°S and 82°N (Winker et al., 2010), and completes 15 orbits a day with a 16 day repeat cycle (Trepte, 2020). The detection sensitivity for weak objects such as aerosols and thin cirrus clouds are better

during the night compared to during the day. This is because the solar background during the day gives more noise in the data. The backscattering for these targets also need to be averaged to be able to detect them. (Winker et al., 2010). Hence, only averaged backscattering night data have been used for this project.

The collected raw data are processed at different levels (0 to 4). The higher the level, the more processed the data are (Hostetler et al., 2006). The level 1b data have been used for this project, and its processing includes finding the geolocation of the data, and calibration of the data (Winker et al., 2009). To go more into detail would be out of the scope of this project, but detailed information can be found in Hostetler et al. (2006). The products of the level 1b data consist of profiles of the attenuated backscattering for the 532 nm perpendicular ($\beta'_{532,\perp}$), total 532 nm ($\beta'_{532,tot}$) , and 1064 nm ($\beta'_{1064,tot}$) channel (Winker et al., 2009).

When sunlight goes through the atmosphere it will either get absorbed, scattered, reflected or transmitted. The scattering is going to be important here since the satellite receives the scattered light. The air molecules scatter light at smaller wavelengths through Rayleigh scattering, while aerosols scatter light at the same wavelengths of visible light through Mie scattering. This is because the size of the aerosol particles is the same size as the wavelengths of visible light. The visible light range is between 400 - 700 nm (Ahrens and Henson, 2016), and that is why CALIPSOs 532 nm channel is favourable to detect aerosols since it is in the middle of the visible light spectra.

2.6 Mathematical Background

When the laser crosses the different layers of the atmosphere some light will scatter back, and some will continue through the atmosphere. Hence, the laser pulse gets attenuated by molecules and aerosols. Consequently, the backscattered signal will be reduced compared to if the signal was not attenuated. On the way back to the satellite, it can get attenuated by the same air-mass again. Hence, to retrieve the true backscattering, the attenuation of the laser needs to be taken into account. This is done with the so called two-way transmission parameter (Friberg et al., 2018; Hostetler et al., 2006), which can be expressed as:

$$T^2(z) = exp\left\{-2\int_0^{r(z)} \left[\sigma_m(r') + \sigma_a(r') + \sigma_{O_3}(r')\right] dr'\right\} = T_m^2 \cdot T_a^2 \cdot T_{O_3}^2 \quad (1)$$

The r is the distance from the satellite to the sample, σ_m is the extinction due to backscattering by molecules, σ_a the extinction due to backscattering by aerosols, and σ_{O_3} the extinction due to absorption by ozone. (Friberg et al., 2018; Hostetler et al., 2006). Consequently, the attenuated backscattering can be calculated with equation 2 below.

$$\beta'(z) = \beta(z)T^2(z) \tag{2}$$

This is the product of the level 1b data which will be used for this project (Hostetler et al., 2006). Usually the attenuation caused by particles are considered negligible, while the attenuation caused by molecules is modelled. However, sometimes the particle attenuation is taken into account, e.g. during volcanic conditions (Friberg et al., 2018). This will be discussed further in section 3.5. The true total backscattering can be divided into the backscattering caused by molecules and aerosols (Hostetler et al., 2006):

$$\beta_{tot} = \beta_m + \beta_a \tag{3}$$

The molecular backscattering β_m is based on models using gridded molecular and ozone number density profiles from GMAO (Global Modeling and Assimilation Office). To be able to analyze the backscattering of aerosols, some parameters are needed, one of them being the scattering ratio. This is the ratio between the total scattering and the molecular scattering (Winker et al., 2009):

$$\mathrm{SR} = \frac{\beta_{tot}}{\beta_m} \tag{4}$$

Hence, if the scattering ratio is large, the scattering from aerosols had a large impact. From equation (3) and (4) the second parameter, aerosol scattering, can be retrieved (Friberg et al., 2018):

$$\mathrm{AS} = \beta_{tot} - \beta_m = (\mathrm{SR} - 1)\beta_m \tag{5}$$

Essentially the equation gives the aerosol backscattering coefficients, using equation 4.

2.7 Aerosol Optical Depth and Radiative Forcing

The aerosol optical depth (AOD) is a dimensionless parameter that measures the total extinction by aerosols in an air column. Essentially, it shows how much sunlight that is blocked by the aerosol particles (NOAA, n.d.). It is defined as the integration of the aerosol scattering coefficient, multiplied with

the so-called lidar ratio (S), over the height of the air column (Friberg et al., 2018). The equation is shown below:

$$\text{AOD(lat)} = \int_{\text{alt}} \beta_a \times \text{S} = \int_{\text{alt}} \sigma_a \tag{6}$$

As previously mentioned, the radiative forcing (RF) is a measure of the net imbalance in radiative energy, with unit W/m^2 (Jacob, 1999). To retrieve the radiative forcing, a rough estimate can be expressed using this relation from Hansen et al. (2005):

$$RF \approx AOD \times (-25) \tag{7}$$

2.8 Historical Eruptions

Thomason et al. (2018) investigated the stratospheric AOD using data from GloSSAC (The Global Space-based Stratospheric Aerosol Climatology) from 1979-2014. They found that the stratospheric AOD at 532 nm after the Pinatubo eruption reached a peak value of 0.22 in the tropics a few months after the eruption ($\sim$ 0.15 in the NH). Their results also show a peak of 0.06 in the tropics after the eruption of El Chichón 1982 ($\sim$ 0.15 in the NH), and approximate AOD between 1997-2010 in the northern hemisphere to fluctuate between 0.003-0.015. Further, table 1 shows the peak AOD, peak RF, Volcanic Explosivity Index (VEI) and sulfur dioxide content after five significant eruptions.

Table 1: The table shows the VEI, approximate amount of sulfur dioxide emitted, approximate peak of stratospheric northern hemispheric AOD, and approximate northern hemispheric peak RF for five significant historical eruptions. The date, coordinates, SO_2 for El Chichón, and VEI was found in Global Volcanism Program (2020)'s database, using the volcano names as keywords.

Volcano[a]	Date[a]	Coordinates[a]	VEI[a]	SO_2 (Tg)	NH AOD	RF (W/m^2)
El Chichón	28 Mar 1982	17°N93°W	5	8[a]	0.15[f]	-3.8[i]
Pinatubo	2 April 1991	15°N120°E	6	18-19[b]	0.15[f]	-4.0[h]
Kasatochi	7 Aug 2008	52°N176°W	4	1.7[c]	0.018[g]	-0.5[i]
Sarychev	11 Jun 2009	48°N153°E	4	1.2[d]	0.022[g]	-0.6[i]
Nabro	13 Jun 2011	13°N42°E	4	1.5[e]	0.016[g]	-0.4[i]

[a]Global Volcanism Program (2020). [b]Guo et al. (2004). [c]Thomas et al. (2011). [d]Haywood et al. (2010). [e]Clarisse et al. (2012). [f]Thomason et al. (2018). [g]Friberg et al. (2018). [h]Kremser et al. (2016). [i]Retrieved from the AOD using equation 7.

3 Method

For this analysis, CALIPSO's level 1b data that contain the total attenuated backscattering at 532 nm have been used to estimate the stratospheric backscattering, scattering ratio, aerosol optical depth (AOD), and radiative forcing (RF), before and after the eruption of Raikoke. The following sections clarify what has been done to retrieve these parameters.

3.1 Retrieving Stratospheric Data

The satellite data from CALIOP were analyzed in MATLAB and a few steps toward retrieving only the stratospheric data were executed. Prior to this the true backscattering had already been retrieved using equation 2 and 1. The molecular (including ozone) transmission parameter was based on modelling, and the aerosol transmission parameter was assumed to be 1. The uncertainties of this will be discussed more in section 3.5. The aerosol scattering had also been retrieved using equation 5.

The raw AS data contained backscattering from both aerosols and clouds (see figure 3a) (Friberg et al., 2018). Hence, a cloud mask containing all cloud pixels was created and applied to the raw data. Clouds in the stratosphere consists of ice crystals which are depolarizing. Therefore, they can be separated from aerosols with the depolarization ratio, which is the ratio between the perpendicular and total backscatter at 532 nm (Vernier et al., 2009). A threshold with depolarization ratio of 0.05 was used to create a matrix containing all cloud pixels. All pixels below thick clouds were also included in the cloud mask, and the mask was expanded to include weak signals at the boundary of the clouds (Friberg et al., 2018). This mask was also created prior to the start of this project, and was in this analysis only applied to the raw data (see figure 3b). Since there is much noise in the backscattering, a mean value of the data was taken over the time dimension for four different time periods.

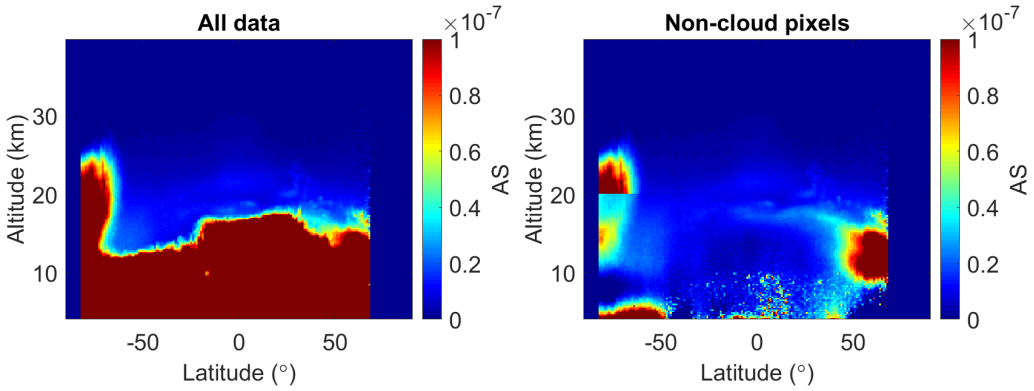

(a) (b)

Figure 3: The figure shows all the mean backscattering data from aerosols and molecules in (a) and only non-cloud data in (b) in the time period 7th of June to 28th of August 2019.

Thereafter, a tropopause mask was created (see figure 4a). This mask was also created prior to this project and applied as a part of this analysis. It was constructed by finding the thermal tropopause using temperature data from MERRA-2 (NASA) corresponding to every CALIPSO orbit. As follows, a matrix was created containing the tropopause mask and then applied to the non-cloud pixel data. With this method, stratospheric aerosol backscattering data were retrieved (see figure 4b).

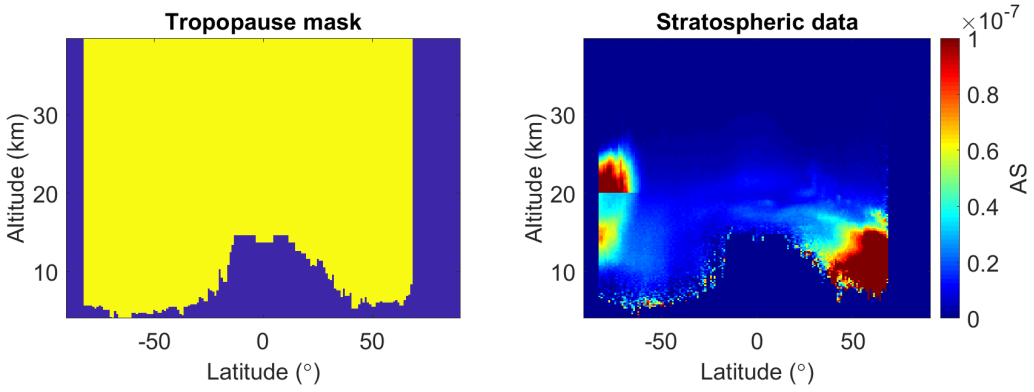

(a) (b)

Figure 4: The figure shows the mean value of the tropopause mask in (a) and the non-cloud stratospheric data with the applied tropopause mask in (b). The mean is taken over the time period 7th of June to 28th of August 2019.

In order to use only stratospheric data originating from the volcanic eruption, a mask to filter out polar stratospheric clouds (PSCs) was created. These clouds form in the winter polar stratosphere and start to form already from 60 °S in the southern hemisphere. They start to form in temperatures below 195 K, so the PSC-mask was created (also prior to this project) with a threshold of that temperature. Data below PSC-clouds were also included in the mask because of the strong attenuation generated by these clouds (Friberg et al., 2018). In the Arctic region, these clouds are not as common since the stratospheric synoptic temperature is warmer than Antarctica due to disruption from planetary waves (Orr et al., 2020). Hence, there were not many PSCs noticed in the winter northern hemisphere. Still, a matrix was created containing these cloud pixels, and applied to the stratospheric data as a part of this analysis. Figure 5 below shows the backscattering data after PSC removal.

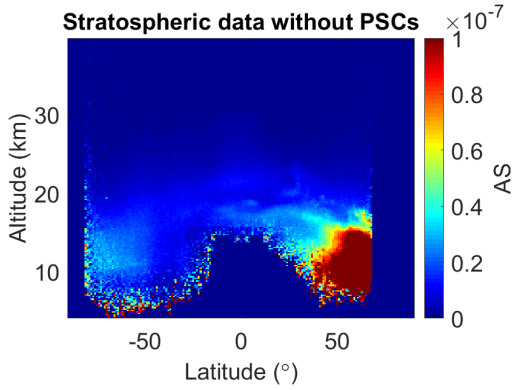

Figure 5: The figure shows the backscattering data from stratospheric particles excluding polar stratospheric clouds. The backscattering data are averaged over the time period 7th of June to 28th of August 2019 as in figure 4.

3.2 Scattering Ratio

Thereafter, the scattering ratio (SR) was calculated using equation (5). The molecular backscattering (β_m) data were modeled prior to this project based on data from GMAO (Friberg et al., 2018), and the aerosol scattering used were the stratospheric data excluding the PSCs. Using this equation, a new 3-D matrix was created with the scattering ratio that was plotted using a scatter plot with the mean value taken over the time dimension. This way the scattering ratio before and after the eruption could be determined and visualized.

When plotting the SR, noise could be detected in the southern hemisphere around 40 °S to 20 °S latitude. This is due to disturbances in Earth's magnetic field called the South Atlantic Anomaly (SAA). It is caused by a drop in the magnetic field which causes cosmic rays and charged particles to extend lower into the atmosphere (Snowden, 2020) . This noise was filtered out by a matrix containing the RMS (root mean square) noise which is measured at high altitudes (60.3-75.3 km) where there is almost no backscattering signal. As a result, the scattering that occurs in this region is mostly a result of background noise (Hostetler et al., 2006). An empirical value of RMS>140 was chosen to filter out the noise due to the SAA. The scattering ratio before and after filtering out the noise can be seen in figure 6a and 6b respectively.

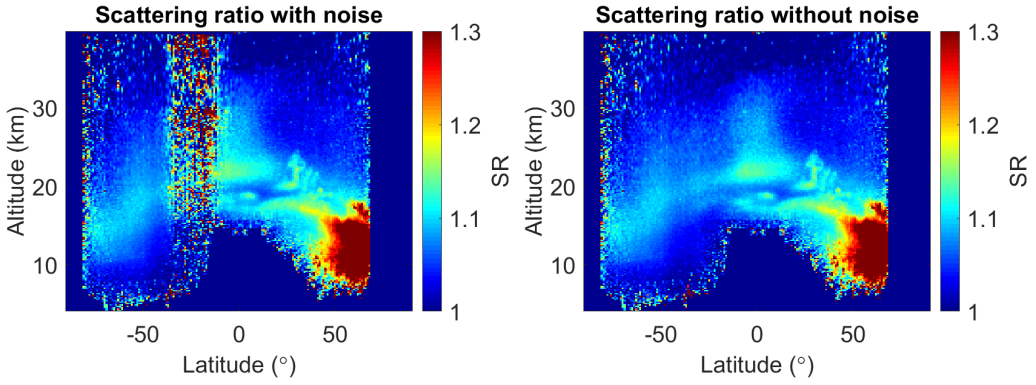

(a) (b)

Figure 6: The figures show the mean scattering ratio over the time period 7th of June to 28th of August with noise (a) and without noise (b).

It should be mentioned that the laser has experienced some low energy laser shots due to decreased pressure inside the canister of the laser. This has caused low and noisy backscattering data in the level 1b product, especially in the SAA area. This is okay since only the northern hemispheric AOD has been analysed in this study. Also, the frequency of these low energy shots has been less than 1% globally (NASA, 2020a).

3.3 Northern Hemisphere Stratospheric Aerosol Optical Depth

Using equation (6), the stratospheric AOD was determined for the northern hemisphere using a lidar ratio of 50 sr, which according to Kremser et al. (2016) is a generally used value for stratospheric aerosols at 532 nm. The

length of every height column was set to 180 m, which is the vertical resolution between 20.2 and 30.1 km (Hostetler et al., 2006). Still, this value was chosen for the entire height column for simplicity. Thenceforth, all the height pixels were added into one value per height column, giving the AOD per latitude and time step.

When computing this (see figure 7a), it could be noticed that data were missing in the polar summer hemisphere since these areas barely contain any night data. This missing data were filled in by extrapolation of the data. Therefore, an algorithm was made to take the mean value of the last six available values and add that value to the remaining higher NaN-latitude data. Since the ratio of the Earth's surface area is only 6 % between 60°S and 90°S (as for the northern hemisphere) (Friberg et al., 2018), this approximation has low impact on the final AOD and RF estimations. Even so, it was necessary to do this extrapolation since the lower Brewer-Dobson branches transport some of the aerosols to the polar regions. Further, the stratosphere is thicker in the polar regions and the AOD can therefore be expected to be higher.

As a last step, the data were area weighted against latitude since each latitude covers different sized areas of the Earth. This was done by taking the AOD per latitude, and multiplying it with the fraction of the Earth that it covers according to the equation below:

$$\mathrm{AOD}_{\mathrm{W,NH}} = \sum_{i=0}^{90} \frac{\mathrm{AOD}(i) \times cos(i)}{\sum_{i=-90}^{90} cos(i)} \tag{8}$$

This was only done for the northern hemisphere since the southern hemisphere was not affected by the eruption. An example with the extrapolated AOD data can bee seen in figure 7b. This data were also smoothed over 8 days which can bee seen in figure 7c.

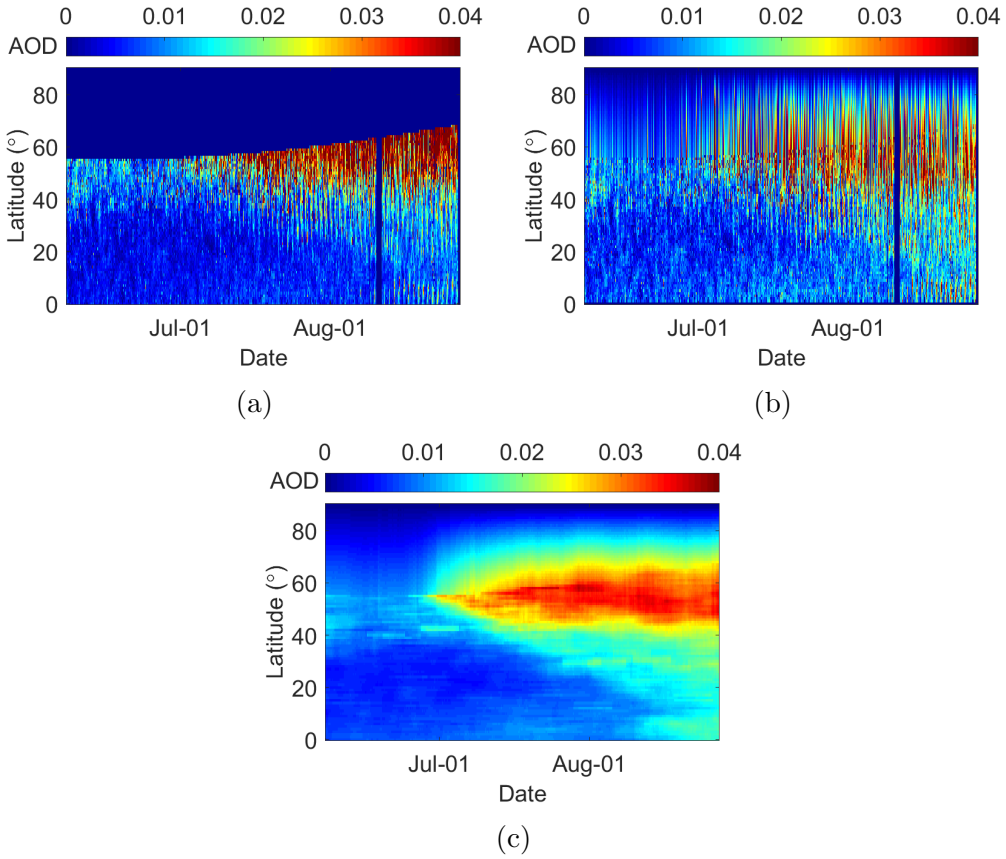

Figure 7: The figures show the AOD in the northern hemisphere during the time period 7th of June to 28th of August without (a) and with (b) extrapolation of the data. Figure (c) shows the smoothing of the data in (b).

3.4 Northern Hemisphere Total Stratospheric Aerosol Optical Depth and Total Radiative Forcing

Lastly, the total stratospheric AOD in the northern hemisphere could be calculated. This is useful to see if the eruption had any effect on the entire northern hemisphere. To do this, the extrapolated and smoothed AOD for all latitudes was added to create a total northern hemispheric AOD for each time swath. Finally, the total radiative forcing in the northern hemisphere was calculated using equation (7), and plotted in the same manner.

3.5 Uncertainties

While retrieving and analyzing data some uncertainties are bound to occur. As discussed before, the attenuation caused by volcanic particles is sometimes taken into account when computing the aerosol transmission parameter T_a^2, which mathematically can lie between 0 - 1. When corrected, the value usually lies between 0.95 - 1. This is because a higher aerosol load leads to higher extinction of the lidar (Friberg et al., 2018). In a study by Friberg et al. (2018), the aerosol attenuation was accounted for which lead to an increase in stratospheric AOD by 4-7 % the first year after the eruptions of Kasatochi, Nabro and Sarychev. Also, when not correcting the aerosol transmission parameter, the SR is usually underestimated in the order of 2 - 5 %. However, implementing this is quite complex, and would be more crucial for volcanic eruptions the size of Pinatubo according to Friberg et al. (2018). Hence, the value of $T_a^2 = 1$ has been chosen to simplify this study.

The chosen value of the lidar ratio (S) can lead to even more uncertainties. The value lies between $\sim$ 40 - 70 sr, and a value of 50 sr is regularly used (Friberg et al., 2018; Kremser et al., 2016). A lower and upper bound when calculating the northern hemispheric AOD have been calculated to show how large the uncertainties become with choosing the frequently used value of 50 sr.

When averaging over many cells, the standard deviation of the mean data decreases. When calculating the mean scattering ratio, not enough cells are averaged to detain a low standard deviation. According to Vernier et al. (2009), averaging over 300 cells for the mean scattering ratio led to a standard deviation of about $\pm$140%. However, averaging over 7200 cells lead to a standard deviation of approximately $\pm$1.6%. Hence, a large standard deviation is expected for the calculation of the mean scattering ratio, but very small for the calculation of the AOD and total AOD (and RF because of proportionality). Therefore, since an extensive amount of pixels are averaged, the standard deviation will become very small for these measurements. The standard deviation may seem large for the mean scattering ratio, but since this is a qualitative measurement with the main goal to analyze the transport and not the concentration of the aerosols, this error is acceptable for this study.

4 Results and Discussion

4.1 Scattering Ratio

The scattering ratio before and after the eruption is shown in figure 8. Figure 8a shows the conditions before the eruption occurred. Still, there are some stratospheric aerosols present in the tropics and in the LMS in the northern hemisphere. Since two-way mixing can occur between the LMS and tropical troposphere, it is not unusual that the LMS already has some background aerosols. The SR in the tropics indicate that there has already been an eruption. In July - October 2018 there were eruptions of the volcano Ambae that is situated in the tropics (Global Volcanism Program, 2019a), which is the reason for the prevailing aerosol concentration in the tropical stratosphere.

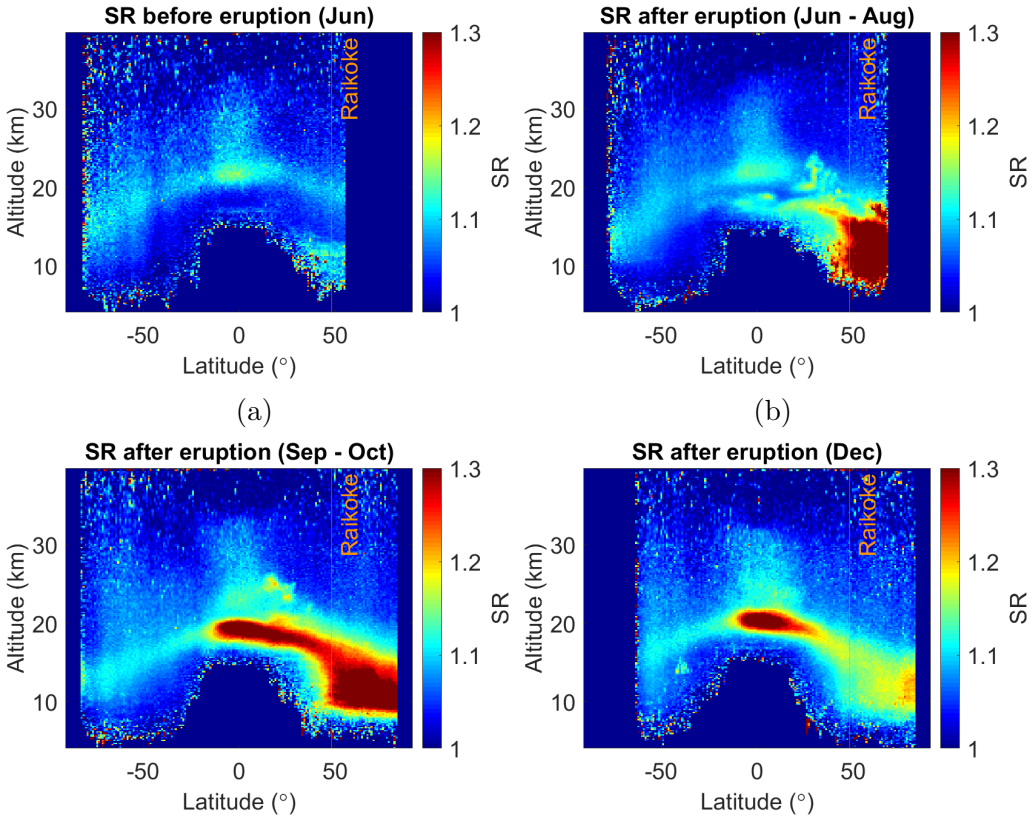

Figure 8: Scattering ratio of the stratosphere between 07/06 - 21/06 (a) 21/06 - 27/08 (b) 30/8 - 31/10 (c) and 01/12 - 31/12 (d) 2019. Data are missing in November and in parts of September.

After the eruption (see figure 8b), a large increase in SR can be observed. This was expected since the ash plumes reached 10-13 km in altitude according to Global Volcanism Program (2019b). However, the SR in figure 8b shows injection to about 18 km altitude, which must mean that the estimation of Global Volcanism Program (2019b) was not that accurate. Hence, the ash plume was directly injected into, and above the LMS, and increased the stratospheric aerosol load. The volcanic aerosols also seem to be located a bit to the north, which was expected since the ash plume drifted north-east after the eruption.

In figure 8c, 3 months after the eruption, it can be noticed that there is a large increase in SR over the tropics, and roughly the same conditions in the extratropics. It can be observed that the aerosols have spread more horizontally, and that the tropics and extratropics is connected with two-way mixing between them. Therefore, the sulfate aerosols from Raikoke have spread to the tropics via the shallow branches in the Brewer-Dobson circulation. Also, the increase could be a result of the tropical eruption of Ulawun. Even if the sulfur dioxide emissions were not as large as Raikoke, some plumes reached 19.2 km straight into the stratosphere (Global Volcanism Program, 2019e), and increased the stratospheric aerosol load. The conclusion is that the increase in the tropics is due to both transport via the Brewer-Dobson circulation, and the eruption of Ulawun.

Approximately six months after the eruption of Raikoke, it can be seen in figure 8d, that much of the stratospheric aerosols in the extratropics have subsided through the tropopause or been transported to the tropics. Since the tropical volcano Ulawun only erupted five days after Raikoke, it could also be remains from this eruption that can be noticed in the tropics. This is reasonable since volcanic particles emitted in the tropics can remain for years in the stratosphere because of the Brewer-Dobson circulation, and volcanic particles emitted in the extratropics subside within a year. Hence, the prevailing stratospheric aerosol load in the tropics is probably a mixture of both eruptions, and the reason for their long residence time the Brewer-Dobson circulation.

In figure 8d, a small increase in SR can be seen around 40°S at approximately 15 km. That is due to some aerosols from the wildfires in southeast Australia that produced an intense period of pyroCb (pyrocumulonimbus) clouds between 29th of December 2019 and 4th of January 2020. These thunderstorm clouds injected aerosols and biomass burning gases straight into the stratosphere, and that is why the SR is increasing in figure 8d (Kablick et al.,

2020). However, since the AOD for the northern hemisphere was analysed, this did not affect the results for this study.

4.2 Aerosol Optical Depth

The latitude weighted, and smoothed stratospheric AOD, is demonstrated in figure 9 for the northern hemisphere. Unfortunately, some time periods miss data, but the change in AOD can still be visualised. The eruption of Raikoke is indicated and it can be seen that an increase of the AOD occurs a few weeks after the eruption. This is because sulfate is what causes an increase in AOD, and it takes some time for it to form in the stratosphere. The greatest increase in AOD arises around 50°N which is reasonable since Raikoke is located at that latitude. On the other hand, because of the horizontal mixing over the isentropic surfaces in the LMS, the max AOD would probably have occurred here no matter where in the extratropics the eruption took place.

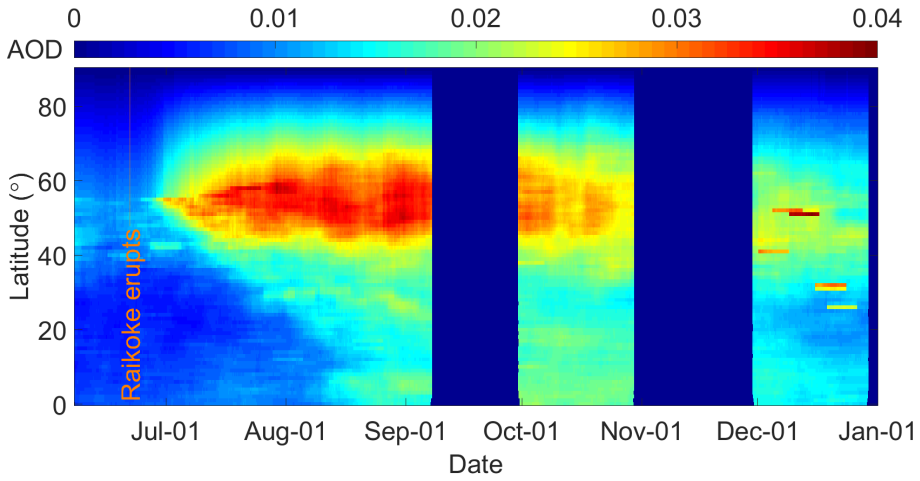

Figure 9: The figure illustrates the stratospheric AOD in the northern hemisphere from 07/06 - 31/12 2019. There can be some remains from clouds in the month of December.

In the beginning of December it can be noted that the AOD has decreased. This is reasonable when comparing to the SR in figure 8d. At that time much of the aerosols have already subsided through the tropopause or been transported to the tropics, and thus will not affect the stratospheric AOD anymore. Still, there is a doubling in AOD from the background conditions before the eruption.

Even though a lot of aerosols can be seen in the tropics in figure 8c and 8d, the AOD is not very strong in the tropics in figure 8. This is because the surface area per latitude is much larger in the tropics than in the mid-latitudes. Thus, the stratospheric aerosols in the tropics cover a much larger area and the same amount of particles does not affect the AOD as much as it would have had in the midlatitudes. Still, some amounts of increase can be seen which is probably because of the tropical Ulawun eruption, and some aerosol transport from the Raikoke eruption to the tropics via the Brewer-Dobson circulation.

Also, the reason for the high SR in figure 8c and 8d in the tropics, is because the SR depends on the surrounding air pressure. Hence, it depends on the amount of air molecules present. The stratospheric SR will therefore be higher in the tropics, because the air pressure is lower, and the larger part of the total extinction will be due to aerosols compared to the midlatitudes. This is due to the thinner stratosphere and higher tropopause in the tropics.

The total northern hemispheric AOD can be seen in figure 10. The black graph represents the total AOD with lidar ratio of 50 sr. The other graphs show the total AOD with lidar ratio of 40 sr (blue) and 70 sr (pink). A value of 70 sr causes the AOD to deviate with 40%, and a value of 40 sr causes the AOD to deviate with 20 %. This shows that the calculation of the AOD is highly dependable on the lidar ratio, and that the broad range of acceptable values induce a high uncertainty in the results. Nonetheless, the proportionality of the increase will be the same for all lidar ratios, and since the goal is to analyse the increase of the stratospheric aerosol load, this is acceptable.

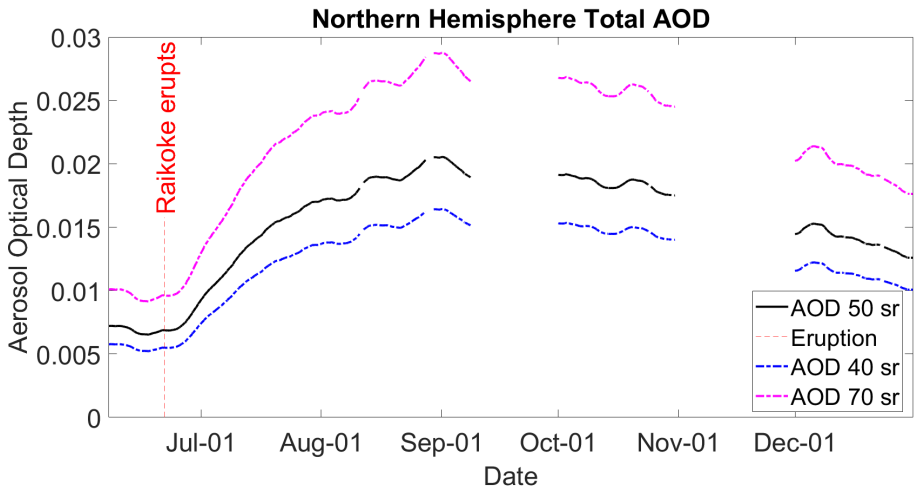

Figure 10: The black graph shows the fluctuation of the northern hemispheric AOD in the stratosphere before and six months after the eruption of Raikoke, with a lidar ratio of 50 sr. The blue graph and pink graph represent the same AOD with lidar ratios of 40 sr and 70 sr respectively.

Figure 10 shows almost a doubling of the stratospheric AOD six months after the eruption. The peak value of the northern hemispheric AOD occurred approximately around the beginning of September and was 0.02. This is very close to the peak value of the eruption of Sarychev (2009) found by Friberg et al. (2018), where the peak northern hemispheric AOD was found to be approximately 0.022, and the AOD went back to normal conditions within a year. This volcano is situated at similar coordinates as Raikoke, and had similar horizontal transport of stratospheric aerosols to the tropics as the Raikoke eruption. Since only six months after the eruption of Raikoke were analysed, it was assumed that the AOD went back to background conditions within a year as the Sarychev eruption because of their similarities. The difference is that the VEI was one value larger (4), and that the amount of sulfur dioxide emitted a bit less (1.2 Tg). The greater amount of sulfur dioxide emitted during the Raikoke eruption ($\sim$ 1.4-1.5 Tg) could therefore be the reason that the stratosphere reached as high AOD values as the Sarychev eruption.

However, unlike Friberg et al. (2018), the attenuation of the particles was not taken into account in this study. This has most likely induced an underestimation of the AOD data. This would explain why the AOD after the Raikoke eruption was similar to that of Sarychev, even though the sulfur dioxide emission was higher after the Raikoke eruption. Since taking the

aerosol attenuation into account led to an increase in stratospheric AOD by 4-7 % after the eruptions of Sarychev, Nabro and Kasatochi in Friberg et al. (2018), it can therefore be assumed that the increase in AOD might have been underestimated by the same amount in this analysis. Hence, the peak AOD might have been the same or even larger than after the eruption of Sarychev.

Comparing with larger eruptions such as El Chichón and Pinatubo in table 1, their peak AOD is approximately 7 times larger than that of the Raikoke eruption. That is most likely because of the large amounts of sulfur dioxide emitted during these eruptions (8 Tg and 18-19 Tg respectively), and that they are situated at the tropics. The location of the eruption influences the effect the eruption has globally. Since the eruption of Raikoke occurred in the midlatitudes (48°N), most of the volcanic aerosols stayed in the LMS, or were transported via the Brewer-Dobson circulation to the tropics, and affected the northern hemispheric AOD. This further shows that the Brewer Dobson circulation inhibits transport between the hemispheres, so eruptions that do not occur in the tropics will only affect the hemispheres where the eruption took place.

4.3 Radiative Forcing

The northern hemispheric radiative forcing, due to elevation of the stratospheric aerosol load, is shown in figure 11. The peak, or rather the minimum value, occurs in the beginning of September, and has a value of -0.5 W/m^2. These values are very similar to the eruptions of Kasatochi (-0.5 W/m^2), Sarychev (-0.6 W/m^2) and Nabro (-0.4 W/m^2) as stated in table 1. Since the radiative forcing is directly related to the AOD using equation 7, the same argument as for why they are similar in the AOD goes for the radiative forcing.

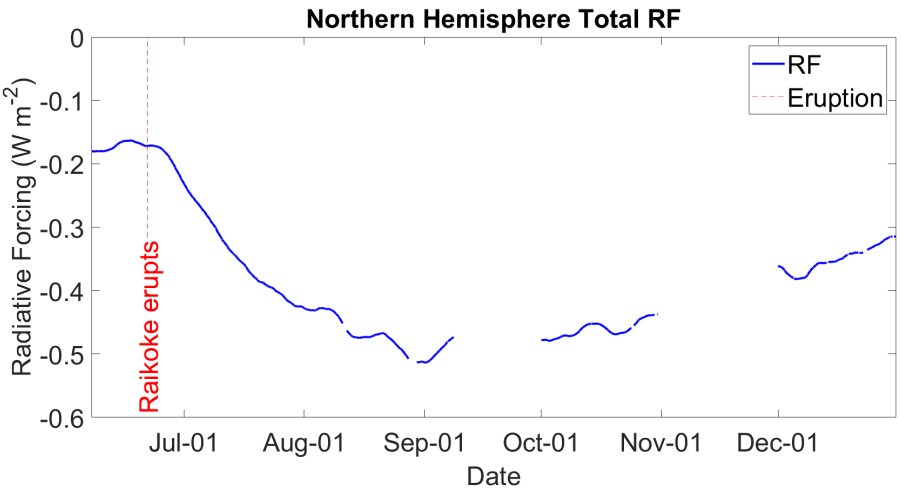

Figure 11: The figure shows the total fluctuation in radiative forcing in the northern hemisphere due to elevation in the stratospheric aerosol load before, and six months after the eruption of Raikoke.

The eruption of Pinatubo had a minimum value of -4 W/m^2 after the eruption, and it is known from e.g. McCormick, Thomason, and Trepte (1995), that the global temperature decreased with 0.5 °C years after the eruption. Since the eruption of Raikoke only emitted around 8 % sulfur dioxide of that of Pinatubo, and also in the midlatitudes, the eruption had probably not a great effect on the global temperature. However, according to Solomon et al. (2011), smaller eruptions between 2000 - 2010 contributed to an increase in the stratospheric background conditions, and this perturbation led to a decrease in global radiative forcing of about -0.1 W/m^2. This indicates that smaller to moderate eruptions such as the one of Raikoke, does have a small, but not negligible, effect on the climate. Most importantly, this further shows that it is important to include this change in the stratospheric aerosol load in climate models to decrease the risk of masking the global warming caused by greenhouse gases.

5 Conclusions

After the eruption of Raikoke, an increase in the stratospheric aerosol load (SR) could be observed. Six months after the eruption, some of the stratospheric aerosol load remained in the LMS, or had been transported to the tropics through the shallow branches of the Brewer-Dobson circulation. The stratospheric aerosol load in the tropics was also affected by emissions from the eruption of Ulawun. A maximum in the stratospheric AOD of 0.02 could be detected roughly three months after the eruption in the northern hemisphere. A minimum value of the radiative forcing of -0.5 W/m^2 was estimated at the same time. The calculation of the AOD has some large uncertainties due to the broad range of lidar ratios, and due to the aerosol attenuation of the lidar, which gives an underestimation of the AOD. However, comparing the AOD and RF to similar volcanic eruptions such as Sarychev, the results seem reasonable and trustworthy. Comparing the stratospheric aerosol load to the Sarychev eruption, it could be assumed that the stratospheric aerosol load went back to background conditions roughly within one year.

Comparing to the global temperature change of the major eruption of Pinatubo in 1991, the eruption of Raikoke presumably did not cause a large global temperature decrease. Nonetheless, since smaller eruptions have been shown to induce a small change in radiative forcing over the decade 2000 - 2010, it can be assumed that the eruption of Raikoke, together with other small to moderate volcanic eruptions, induce a small change in radiative forcing. Thus, the eruption has most likely contributed to a slow down of the global warming caused by greenhouse gases.

6 Outlook

This study has proved further that minor eruptions can affect the stratospheric aerosol load. Future studies should continue to study upcoming volcanic eruptions to be able to use the results in climate models. Further studies analysing the lidar ratio should also be executed to avoid errors in calculating the AOD. Additionally, calculations as how to include the attenuation of the laser caused by aerosols should be included to avoid underestimation of the AOD. This was not done due to the time limitation of this study, but can be done for future work. Also, modelling to retrieve the radiative forcing should be carried out to get as a precise result as possible. Different instruments such as ground based lidars or aircraft measurements could also be used for future work to be able to compare different types of data.

References

Ahrens, C. D. and R. Henson (2016). *Meteorology Today - An introduction to Weather, Climate, and the Environment*. 11th ed. Boston: Cengage Learning.

Andersson, Sandra M. et al. (2015). "Significant radiative impact of volcanic aerosol in the lowermost stratosphere". In: *Nature Communications* 6.7695. DOI: https://doi.org/10.1038/ncomms8692.

Birner, T. and H. Bönisch (2011). "Residual circulation trajectories and transit times into the extratropical lowermost stratosphere". In: *Atmos. Chem. Phys.* 11, pp. 817–827. DOI: DOI:10.5194/acp-11-817-2011.

Butchart, Neal (2014). "The Brewer-Dobson circulation". In: *Rev. Geophys.* 52.2, pp. 157–184. DOI: 10.1002/2013RG000448.

Clarisse, L. et al. (2012). "Retrieval of sulphur dioxide from the infrared atmospheric sounding interferometer (IASI)". In: *Atmos. Meas. Tech.* 5.D12, pp. 581–594. DOI: DOI:10.5194/amt-5-581-2012.

Friberg, Johan et al. (2018). "Volcanic impact on the climate – the stratospheric aerosol load in the period 2006–2015". In: *Atmospheric Chemistry and Physics* 18.15, pp. 1149–11169. DOI: 10.5194/acp-18-11149-2018.

Global Volcanism Program (2013). *Raikoke (290250)*. [Online] Last updated: 17 September 2020. Available at: URL: https://volcano.si.edu/volcano.cfm?vn=290250. [Accessed 24 September 2020].

— (2019a). "Report on Ambae (Vanuatu) (Crafford, A.E., and Venzke, E., eds.)" In: *Bulletin of the Global Volcanism Network* 44.6. Smithsonian Institution. DOI: DOI:10.5479/si.GVP.BGVN201906-257030.

— (2019b). "Report on Raikoke (Russia)". In: *Sennert, S K (ed.), Weekly Volcanic Activity Report, 19 June-25 June 2019* Smithsonian Institution and US Geological Survey. URL: https://volcano.si.edu/showreport.cfm?doi=GVP.WVAR20190619-290250. [Accessed 24 September 2020].

— (2019c). "Report on Raikoke (Russia) (Crafford, A.E., and Venzke, E., eds.)" In: *Bulletin of the Global Volcanism Network* 44.8. Smithsonian Institution. DOI: DOI:10.5479/si.GVP.BGVN201908-290250.

— (2019d). "Report on Ulawun (Papua New Guinea) (Bennis, K.L., and Venzke, E., eds.)" In: *Bulletin of the Global Volcanism Network* 44.12. Smithsonian Institution. DOI: DOI:10.5479/si.GVP.BGVN201912-252120.

— (2019e). "Report on Ulawun (Papua New Guinea) (Venzke, E., ed.)" In: *Bulletin of the Global Volcanism Network* 44.9. Smithsonian Institution. DOI: DOI:10.5479/si.GVP.BGVN201909-252120.

Global Volcanism Program (2020). *Database Search - Volcano Search.* [Online] Available at: URL: https://volcano.si.edu/search_volcano.cfm. [Accessed 2 December 2020].

Guo, S. et al. (2004). "Re-evaluation of SO2 release of the 15 June 1991 Pinatubo eruption using ultraviolet and infrared satellite sensors". In: *Geochemistry, Geophysics, Geosystems* 5.4. DOI: DOI:10.1029/2003GC000654.

Hansen, J. et al. (2005). "Efficacy of climate forcings". In: *J. Geophys. Res.-Atmos.* 110, p. D18104. DOI: DOI:10.1029/2005JD005776.

Haywood, J.M. et al. (2010). "Observations of the eruption of the Sarychev volcano and simulations using the HadGEM2 climate model". In: *J. Geophys. Res.-Atmos.* 115.D12, pp. 1–18. DOI: DOI:10.1029/2010JD014447.

Holton, J. R. et al. (1995). "Stratosphere-troposphere exchange". In: *Reviews of Geophysics* 33.4, pp. 403–439. DOI: 10.1029/95RG02097.

Hostetler, C. A. et al. (2006). *CALIOP Algorithm Theoretical Basis Document - Calibration and Level 1 Data Products, PC-SCI-201 Release 1.0,* [pdf] NASA. Available at: URL: https://www-calipso.larc.nasa.gov/resources/pdfs/PC-SCI-201v1.0.pdf. [Accessed: 19 November 2020].

IPCC (2013). "Climate Change 2013: The Physical Science Basis. Contribution of Working Group I to the Fifth Assessment Report of the Intergovernmental Panel on Climate Change [Stocker, T.F., D. Qin, G.-K. Plattner, M. Tignor, S.K. Allen, J. Boschung, A. Nauels, Y. Xia, V. Bex and P.M. Midgley (eds.)]" In: Cambridge University Press, Cambridge, United Kingdom and New York, NY, USA, 1535 pp. DOI: 10.1017/CBO9781107415324.

Jacob, D. J. (1999). *Introduction to Atmospheric Chemistry.* [e-book] Princeton University Press. Chap. 7. URL: http://acmg.seas.harvard.edu/publications/jacobbook/bookchap7.pdf. [Accessed 11 December 2020].

Kablick, G. P. et al. (2020). "Australian PyroCb Smoke Generates Synoptic Scale Stratospheric Anticyclones". In: *Geophysical Research Letters* 47.13, pp. 1–9. DOI: 10.1029/2020GL088101.

Kremser, Stefanie et al. (2016). "Stratospheric aerosol—Observations, processes, and impact on climate". In: *Rev. Geophys.* 54.2, pp. 278–335. DOI: 10.1002/2015RG000511.

McCormick, M. P., L. W. Thomason, and C. R. Trepte (1995). "Atmospheric effects of the Mt Pinatubo eruption". In: *Nature* 373, pp. 399–404. DOI: DOI:10.1038/373399a0.

NASA (2020a). *CALIPSO Low Laser Energy Technical Advisory for Data Users.* [Pdf] Available at: URL: https://www-calipso.larc.nasa.gov/resources/calipso_users_guide/advisory/advisory_2018-

06-12/CALIPSO_Laser_Energy_Technical_Advisory.pdf. [Accessed 3 December 2020].

NASA (2020b). *NASA Worldview*. [Online] Available at: URL: https://worldview.earthdata.nasa.gov/?v=14.703632130524824,10.253675255552082,236.6460112269132,110.47453081626496&t=2019-06-29-T00%5C%3A00%5C%3A00Z&l=OrbitTracks_Calipso_Descending,OrbitTracks_Calipso_Ascending,AIRS_Prata_SO2_Index_Day(hidden),AIRS_Prata_SO2_Index_Night,Reference_Features,Coastlines(hidden),MODIS_Terra_CorrectedReflectance_TrueColor(hidden),VIIRS_SNPP_CorrectedReflectance_TrueColor(hidden),MODIS_Aqua_CorrectedReflectance_TrueColor(hidden). [Accessed 12 December 2020].

Neely, R. R. et al. (2013). "Recent anthropogenic increases in SO_2 from Asia have minimal impact on stratospheric aerosol". In: *Geophys. Res. Lett.* 40.5, pp. 999–1004. DOI: DOI:10.1002/grl.50263.

Newhall, C. G. and S. Self (1982). "The Volcanic Explosivity Index (VEl): An Estimate of Explosive Magnitude for Historical Volcanism". In: *J. Geophys. Res.* 87.C2, pp. 1231–1238. DOI: DOI:10.1029/JC087iC02p01231.

NOAA (n.d.). *SURFRAD Aerosol Optical Depth*. [Online] Available at: URL: https://www.esrl.noaa.gov/gmd/grad/surfrad/aod/#:~:text=An$%5C%$20aerosol$%5C%$20optical$%5C%$20depth$%5C%$20product,absorbing$%5C%$20or$%5C%$20by$%5C%$20scattering$%5C%$20light. [Accessed: 14th of September 2020].

Orr, A. et al. (2020). "Polar stratospheric clouds initiated by mountain waves in a global chemistry–climate model: a missing piece in fully modelling polar stratospheric ozone depletion". In: *Atmos. Chem. Phys.* 20.21, pp. 12483–12497. DOI: DOI:10.5194/acp-20-12483-2020.

Plumb, R. A. (2002). "Stratospheric Transport". In: *Journal of the Meteorological Society of Japan* 80.4B, pp. 793–809. DOI: 10.2151/jmsj.80.793.

Ramanathan, V. and Y. Feng (2008). "On avoiding dangerous anthropogenic interference with the climate system: Formidable challenges ahead". In: *PNASk* 105.38, pp. 14245–14250. DOI: DOI:10.1073/pnas.0803838105.

Sheng, J. et al. (2015). "Global atmospheric sulfur budget under volcanically quiescent conditions: Aerosol-chemistry-climate model predictions and validation". In: *Geophys. Res. Atmos.* 120.1, pp. 256–276. DOI: 10.1002/2014JD021985.

Snowden, S. L. (2020). *South Atlantic Anomaly*. [Online] Last updated: 25 August 2020. Available at: URL: https://heasarc.gsfc.nasa.gov/docs/rosat/gallery/misc_saad.html. [Accessed 1 December 2020].

Solomon, S. et al. (2011). "The Persistently Variable "Background" Stratospheric Aerosol Layer and Global Climate Change". In: *Science.* 333.6044, pp. 866–870. DOI: 10.1126/science.1206027.

Thomas, H. E. et al. (2011). "A comparison of AIRS, MODIS and OMI sulphur dioxide retrievals in volcanic clouds". In: *Geomatics, Natural Hazards and Risk* 2:3, pp. 217–232. DOI: DOI:10.1080/19475705.2011.564212.

Thomason, L. W. et al. (2018). "A global space-based stratospheric aerosol climatology: 1979–2016". In: *Earth Syst. Sci. Data* 10.1, pp. 469–492. DOI: DOI:10.5194/essd-10-469-2018.

Trepte, C. R. (2020). *A-Train Constellation.* [Online] Last updated: 2 December 2020. Available at: URL: https://www-calipso.larc.nasa.gov/about/atrain.php. [Accessed 9 December 2020].

Vernier, J. P. et al. (2009). "Tropical stratospheric aerosol layer from CALIPSO lidar observations". In: *J. Geophys. Res.* 114.D00H10. DOI: DOI:10.1029/2009JD011946.

Winker, D. M. et al. (2010). "The CALIPSO Mission - A Global 3D View of Aerosols and Clouds". In: *Bull. Amer. Meteor. Soc.* 91.9, pp. 1211–1230. DOI: 10.1175/2010BAMS3009.1.

— (2009). "Overview of the CALIPSO Mission and CALIOP Data Processing Algorithms". In: *Journal of Atmospheric and Oceanic Technology* 26.11, pp. 2310–2323. DOI: DOI:10.1175/2009JTECHA1281.1.